In: **NEUROSCIENCE** 268: pp. 87-101. (2014)
doi.org/10.1016/j.neuroscience.2014.03.006

POTASSIUM CHANNELS IN THE CENTRAL NERVOUS SYSTEM OF THE SNAIL, *HELIX POMATIA*: LOCALIZATION AND FUNCTIONAL CHARACTERIZATION

Izabella Battonyai, Nóra Krajcs, Zoltán Serfőző, Tibor Kiss and Károly Elekes*

Department of Experimental Zoology, Balaton Limnological Institute, MTA Centre for Ecological Research, Hungarian Academy of Sciences, H-8237 Tihany, Hungary

*Corresponding author. Tel. +3687448244/103 ext.
e-mail: elekes.karoly@okologia.mta.hu (K. Elekes)

Abbreviations: BSA, bovine serum albumin; DAB, 3,3'-diaminobenzidine; IHC, immunohistochemistry; PB, phosphate buffer; PBS, phosphate buffered saline; PC, procerebrum; TBS, Tris-buffered saline; TEA, tetraethylammonium-chloride

Abstract

The distribution and functional presence of three voltage-dependent potassium channels, $K_v2.1$, $K_v3.4$, $K_v4.3$, respectively, were studied in the central nervous system of the snail *Helix pomatia* by immunohistochemical and electrophysiological methods. Cell clusters displaying immunoreactivity for the different channels were observed in all parts of the CNS, although their localization and number partly varied. Differences were also found in their intracellular, perikaryonal and axonal localization, as well as in their presence in non-neuronal tissues nearby the CNS, such as the perineurium and the aorta wall. At ultrastructural level $K_v4.3$ channel immunolabeling was observed in axon profiles containing large 80-100 nm granular vesicles. Blotting analyses revealed specific signals for the $K_v2.1$, $K_v3.4$ and $K_v4.3$ channels, confirming the presence of the channels in the *Helix* CNS. Voltage clamp recordings proved that outward currents obtained from neurons displaying $K_v3.4$ or $K_v4.3$ immunoreactivity contained transient components while $K_v2.1$ immunoreactive cells were characterized by delayed currents. The distribution of the K^+-channels containing neurons suggests specific roles in intercellular signaling processes in the *Helix* CNS, most probably related to well-defined, partly local events. The cellular localization of the K^+-channels studied supports their involvement in both pre- and postsynaptic events at perikaryonal and axonal levels.

Keywords: potassium channels – localization – immunohistochemistry – electrophysiology – CNS – snail, *Helix*

1. Introduction

Potassium (K^+) channels are the most widely distributed type of ion channels which can be found virtually in all living organisms (Kurachi et al., 1999). Voltage-dependent K^+-channels are complex proteins composed of six trans-membrane segments, and this building block constitutes the basic pore-forming unit of most eukaryotic voltage-gated K^+-channels (Choe, 2002). The functional channel is formed in the membrane by the assembly of four of the six subunits. Early studies have identified four members of the voltage-dependent K^+-channel family, the K_v1, K_v2, K_v3, K_v4 channels which correspond to the *shaker*, *shab*, *shaw* and *shal* channel subfamilies, respectively, originally identified in *Drosophila* (Butler et al., 1989). Studies with mammals have revealed a number of additional channel varieties (K_v5-12, Kues and Wunder, 1992). K^+-channels have already been identified in the egg of coelenterates (Hagiwara et al., 1981). The diversification of the K^+-channels started by the early evolution of metazoan animals and since they have developed an extraordinary molecular diversity (Birnbaum et al., 2004). In invertebrates K^+-channels represent the largest channel family, including about 30 identified genes in flies and 90 genes in worms (Butler et al., 1989; Wei et al., 1996; Kurachi et al., 1999).

Voltage-dependent K^+-channels play a pivotal role in bursting of nerve cells and neuronal excitability (Hille, 2001; Migliore and Shepherd, 2002; Frick and Johnston, 2005; Vacher, 2008), as well as they stabilize cell voltages by counteracting the depolarizing effect of other (Ca^{2+} and Na^+) channels and re-polarize cells following action potentials (Conley and Brammar, 1999). In nerve cells various K^+-channels have also been shown to participate in synaptic plasticity for short- and long-term memory, meanwhile they can be activated or suppressed depending on function and physiological effects (Pfaffinger and Siegelbaum, 1990).

A voltage-dependent rectifying K^+-channel was first described 60 years ago in the giant axon of the squid (Hodgkin and Huxley, 1952) and later K-current was recorded from neurons of the slug *Onchidium* by Hagiwara et al. (1961). The cloning of *Aplysia* K^+-channel showed a considerable homology to other K^+-channels cloned in vertebrates (Pfaffinger et al., 1991), and a *shaker* K^+-channel gene has been demonstrated to influence the electrical properties of identified *Aplysia* neurons (Kaang et al., 1992). The role of K^+-channels in the modification of learning processes in *Aplysia* (Kandel and Schwartz, 1982; Baxter and Byrne, 1990) and *Hermissenda* (Alkon et al., 1985; Collin et al., 1988) was also demonstrated.

Recently, the contribution of Na^+- and K^+-channels to the function of procerebral globuli cells has been suggested in *Helix pomatia* (Pirger et al., 2013). Azanza et al. (2008) demonstrated the presence of different ion channels, including the delayed rectifier K^+-channel, in the neurons of the subesophageal ganglion complex of *Helix aspersa* by immunohistochemistry. However, the investigation of other the voltage-gated channels as well as the precise distribution, projections and possible intercellular contacts of K^+-channel containing neurons have been neglected completely. Data have also been missing regarding the presence, distribution and cellular localization of K^+-channels in the rest of the snail CNS, including the pairs of the buccal, cerebral (brain) and pedal ganglia, which contain pivotal elements and networks involved in the regulation of different physiological processes such as feeding and locomotion and learning phenomena connected to them (Chase, 2002). The precise localization and functional characterization of K^+-channels are indispensable to have a better insight in K^+-channels regarding their possible implication in signal transduction processes in the nervous system of gastropods, a group including important models of neurobiology.

In order to obtain information as broad as possible on the presence of voltage-gated K^+-channels in the *Helix* CNS, we have tested several, altogether seven antibodies raised against

different K^+-channels. First it was the K_v1 family ($K_v1.1$, $K_v1.2$, $K_v1.4$) because *shaker* related genes generally show a high degree of interspecies conservation (Wymore et al., 1994). Then we also investigated the $K_v4.2$ and $K_v4.3$ channels because they are often co-expressed (Kollo et al., 2006), as well as we have selected $K_v3.4$ and $K_v2.1$ representing other family members. Since $K_v2.1$, $K_v3.4$ and $K_v4.3$ antibodies provided unequivocal and consequent immunolabeling, the distribution and localization of these three voltage-dependent potassium channel were analyzed in details in the CNS of *Helix pomatia*. Blotting experiments were made in order to prove the specificity of the presence of the channels demonstrated immunohistochemically. Finally, using electrophysiological (voltage clamp) methods we have proved the functional presence of the three voltage-dependent K^+-channels in nerve cells displaying the corresponding immunolabeling. Preliminary data on the immunohistochemical localization of the $K_v4.3$ channel has been published (Battonyai et al., 2012).

2. Experimental procedures

2.1 Animals

Adult specimens of the snail *Helix pomatia* were used. They were collected in the surrounding areas of Tihany, kept until use under laboratory conditions and fed on lettuce.

2.2 Immunohistochemistry

2.2.1 Light microscopic immunohistochemistry

For immunohistochemistry (IHC) the buccal and cerebral ganglia as well as the suboesophageal ganglion complex were dissected and fixed in 4% paraformaldehyde diluted

in 0.1 M phosphate buffer (PB, pH 7.4) for 5 hours at 4 °C. Following incubation overnight at 4 °C in PB containing 20% sucrose, 14-16 μm cryostat sections were cut and placed on chrome-alum gelatin coated slides. The cryostat sections were washed for 30 minutes in phosphate-buffered saline (PBS) containing 0.25% TX-100 (PBS-TX) at room temperature. Non-specific binding sites were blocked for 30 minutes by adding 0.25% bovine serum albumin (BSA) to PBS-TX. The following primary antibodies were used: polyclonal anti-K_v3.4 (1:500, Alomone Labs, epitope: peptide EAGDD ERELA LQRLG PHEG(C), corresponding to residues 177-195 of rat K_v3.4, intracellular, N-terminal part) and anti-K_v4.3 (1:1000; Alomone Labs, epitope: peptide (C)NEALELTGTPEEEHMGK, corresponding to amino acid residues 451-468 of human K_v4.3, intracellular, C-terminus), and monoclonal mouse anti-K_v2.1 antibody (1:500; Neuromab Antibodies Inc., epitope: synthetic peptide amino acids 221-229 (LPELQSLDEFGQSTDNPQL, extracellular S1-S2 loop) of rat K_v2.1) .

After washing three times in PBS-TX, the sections were incubated either with rabbit anti-donkey IgG conjugated with TRITC or FITC (1:200; Dako), or with biotin-conjugated goat anti-mouse IgG or anti-rabbit IgG (1:200; Vector Laboratory), depending on the primary antibody. It was followed by avidin-HRP labeling for 1 hour (1:200; Vector Laboratory). All antisera were diluted in PBS-TX-BSA and the incubations lasted for 24 hours at 4 °C, but for the biotin-conjugated IgGs with 5 hours and for avidin-HRP with 3 hours at room temperature. The HRP reaction was visualized in 0.1 M Tris-HCl buffer (TB) (pH 7.6) by adding 0.05% 3’3-diaminobenzidine (DAB, Sigma, St. Louis, MO) as chromogen and 0.01% H_2O_2 as substrate. The development was monitored under a stereomicroscope, and after washing in PBS, the sections were mounted in 1:1 mixture of glycerin-PBS and viewed in a Zeiss Axioplan compound microscope attached to a CCD camera (Alpha DCM510, Hangzhou Scopetek Opto-Electric). All immunohistochemical experiments were repeated at least three times and for each experiment at least five CNS were used.

The specificity of each antibody was tested by applying both method and pre-adsorption control experiments. In case of method control, BSA was used instead of primary antibody or the primary antibody was omitted. In preabsorption control experiments, the diluted antibodies were incubated with their appropriate antigen (1 μg peptide/1 μg antibody; K_v3.4, K_v4.3, Alomone Labs; K_v2.1, Neuromab Antibodies Inc.) overnight at 4 °C prior to the treatment of the cryostat sections. No immunostaining could be observed following these control experiments.

2.2.2 Correlative light-and electron microscopy

In case of K_v4.3 channel correlative light-and electron microcopy was performed as follows. Following fixation overnight at 4 °C in the mixture of 4% paraformaldehyde and 0.1% glutaraldehyde diluted in PB, the procerebrum (PC) from the cerebral ganglia and the caudo-medial lobe from the pedal ganglia were dissected and embedded in a mixture of 10% gelatin and 1% albumin. Fifty μm thick slices cut with a Vibratome (Pelco) were processed for two-step immunocytochemistry. After blocking PBS-TX-BSA and then in 1% H_2O_2, the slices were incubated with anti-rabbit K_v4.3 antiserum, followed by a treatment with a one-step polymer-HRP IHC Detection System (BioGenex). Both antisera were diluted PBS-BSA-TX and the incubation lasted overnight at 4 °C. After washing in PBS and 0.1 M Tris-HCl buffer, the immunoreactions were visualized as described above. The slices were then post-fixed in 0.5% OsO_4 diluted in 0.1 M cacodylate buffer for 30 minutes at 4 °C, dehydrated in graded ethanol and propylene oxide. Block staining was performed in 70% ethanol saturated with uranylacetate. After dehydration the slices were mounted on slides in Araldite (Durcupan ACM, Fluka), and following polymerization they were analyzed in a Zeiss Axioplan compound light microscope. Slices displaying high quality of immunolabeling were selected and re-embedded for electron microscopy. Ultrathin sections of 60–70 nm were cut on an

LKB Novacut ultramicrotome, stained with lead citrate and viewed in a JEOL 1200EX electron microscope.

2.3 Western blot experiments

2.3.1 K_v2.1, K_v3.4 and K_v4.3 Western blots

For K_v2.1 and K_v3.4 immunoblotting ten pieces of the CNS including the surrounding neural sheath or ten pieces of PC, meanwhile for K_v4.3 immunoblotting ten pieces of desheathed CNS, separated connective tissue sheath and PC, respectively, were homogenized in an SDS-containing lysating buffer. PC and CNS were used separately because PC, which is the olfaction center is a completely different unit of the CNS regarding its cellular organization. Since K_v4.3 channel showed strong immunolabeling in the connective tissue sheath it was also tested separately in these experiments. Electrophoresed proteins were blotted onto nitrocellulose membranes and after washing in 0.1 M Tris-HCl buffer with 0.1% Tween-20 (TBS-T) pH (7.6) membranes were blocked by 5% non-fat milk. Then membrane strips were incubated with anti-K_v2.1 antiserum (1:200), anti-K_v3.4 (1:200) or anti-K_v4.3 (1:200) antiserum at 4 °C overnight. After washing in 0.1 M TBS-T (pH 7.6) membrane strips were incubated with a HRP-conjugated goat anti-mouse antibody (Sigma, 1:5000) in case of K_v2.1 antibody and HRP-conjugated goat anti-rabbit antibody (Dako, 1:2000) in case of K_v3.4 and K_v4.3 antibody for 1 hour at room temperature. After washing in 0.1 M TBS-T (pH 7.6) and in 0.1 M TBS the visualization of the reaction product was carried out with ECL reagent (Pierce), or in Tris-HCl buffer (pH 7.6) containing 0.05% DAB (Sigma) as chromogen and 0.01% H_2O_2 as substrate. Method control experiments were performed by omitting the primary antibody and preabsorption specificity control was made with the recognizing

peptides (1 µg peptide/ 1 µg antibody). No labeled bands could be detected following these control experiments.

2.4 Electrophysiology

Electrophysiological experiments were made on neurons of the adult *Helix* CNS selected from those expressing immunolabeling against K_v4.3 (pedal ganglion, caudo-medial lobe neurons, see Figs. 4E, 5), K_v2.1 (cerebral ganglion, PC; see Figs. 1D, 5), and K_v3.4 (buccal ganglion, B2 cell; see Fig. 5) channels, respectively. PC cells were selected as being identified for their role in odor information processing (Gelperin, 1999) and the B2 neuron was identified previously innervating and regulating the salivary gland (Altrup and Speckmann, 1982). Finally, we have chosen the caudo-medial neurons in the pedal ganglion for the K_v4.3 (A-type) current recording because of their clear localization and size.

The cerebral, pedal and buccal ganglia were dissected from the animal, pinned out in a Sylgard-coated dish, and the thick connective tissue sheath was removed. The innermost perineurium was digested by a treatment with 1% protease (Sigma XIV, Sigma) for 5-8 minutes. Current recordings from the large size neuron located in the buccal ganglia were performed using a GeneClamp amplifier (Axon Instruments, Union City, USA) in two microelectrode voltage-clamp (VC) mode. Currents from small diameter neurons located in the PC and the pedal ganglia were recorded using an AxoClamp 2B amplifier in discontinuous SEVC mode. Electrodes pulled from borosilicate glass capillaries (1B1150F-3 World Precision Instrument, Inc., Sarasota, USA) had a resistance of 4–6 MΩ when filled with Na-acetate (4 mM) or KCl (2.5 mM) solution. Data acquisition and analysis were performed using Digidata interface and pCLAMP software (Axon Instruments). Capacity and leakage subtraction were performed using a combination of analogue compensation and P/24

subtraction protocol. Experiments were performed at room temperature of 20-22 ^{o}C in snail physiological solution in mM: 80 NaCl, 4 KCl, 10 $CaCl_2$, 5 $MgCl_2$, 10 Tris-HCl, (pH=7.4). The recording chamber (0.5 ml) was perfused continuously at a rate of 1 ml/min with snail physiological solution using a gravity feeding system and the superfluous solution was removed by suction. In part of the experiments for recording transient outward K-current the physiological solution was modified to contain 5 mM tetraethylammonium chloride (TEA, Sigma, Budapest) and NaCl was replaced for sucrose. In sucrose and 5 mM TEA saline the Na-dependent inward current and part of the K-currents, except A-current, was eliminated.. The large bore pipette (20 mm) was placed close to the cell soma to be studied. The test solution flow from this pipette was controlled changing the hydrostatic pressure applied to the pipette. The use of this superfusion system allowed a rapid and complete change of the local solution with minimal cell disturbance. The following drugs were used: 100nM blood-depressing substance (BDS-II), apamine (not shown), (both from Alomone Labs, Jerusalem), 4mM 4-aminopyridine (4-AP) and 20 mM tetraethylammonium chloride (TEA, both from Sigma, Budapest).

3. Results

3.1 Immunohistochemical localization of K^+-channel containing neurons

Immunohistochemical experiments revealed a broad distribution but at the same time distinct localization of neurons displaying immunoreactivities against $K_v2.1$, $K_v3.4$ and $K_v4.3$ channels, respectively, throughout in the CNS of *Helix* (Figs. 1, 3-5). Although slight differences in the number of labeled cells and cell groups and their localization in the different ganglia could be observed, in general the distribution of the different channel expressing cells

was similar (Fig. 5). The vast majority of the immunolabeled neurons were of small size (5-8 μm or 15-30 μm), meanwhile no large (70-90 μm) or giant (over 100 μm) cells displayed labeling but one (B2) in the buccal ganglia.

3.1.1 $K_v2.1$ channel immunoreactive neurons

$K_v2.1$ immunoreactive (IR) neurons were found in the buccal and cerebral ganglia as well as in the suboesophageal ganglion complex of the *Helix* CNS (Fig. 5). In the medial region of the rostro-dorsal surface of the buccal ganglia they formed a large cluster of the labeled neurons with an average diameter of 15 μm (Fig. 1A, B). In the cerebral ganglion $K_v2.1$-IR globuli cells occurred throughout the cell body layer of the procerebrum (PC; Fig. 1C, D). At higher, immersion oil magnification it could be clearly seen that the strong immunoreactivity was distributed evenly in the narrow cytoplasmic ring of the globuli cells measuring an average diameter of 5-8 μm (Fig. 1D, insert). No labeling was found in the larger (12-15 μm) neurons of the PC located along the marginal surface. In the lateral part of the metacerebrum small bundles of fibers were running, displaying varicose arborizations in the pedal lobe (Fig. 1C). These fibers were found to originate from small (15-20 μm) neurons located within the lobe (Fig. 1E). In the mesocerebrum a group of neurons displayed moderate $K_v2.1$ immunoreactivity (Fig. 1F). Camera lucida drawings revealed further details of the distribution of $K_v2.1$-IR elements in the in the cerebral ganglion (Fig. 2). At low magnification the ruling element was a labeled thick axon bundle system crossing the neuropil in the meso- and metacerebrum and projecting towards the commissure (Fig. 2A), meanwhile high magnification reconstruction provided evidence for the presence of small immunolabeled varicosities located among and around unlabeled neurons in the cell body layer of the PC (Fig. 2C). In the suboesophageal ganglion complex all ganglia contained labeled cell clusters (Fig. 5). The labeled neurons displayed immunoreaction sometimes only in a part of the cytoplasm (Figs. 1G, H). In the parietal ganglia two major groups of labeled neurons were

present, one population formed by smaller size (15-20 μm) cells, located near the pallial nerve root which contained densely arranged labeled axons (Fig. 1G), and the second one contained medium size (40-50 μm) neurons located near the pleural ganglion. Four labeled cell groups were present in the anterior, lateral and medial parts of the perikaryonal layer of the pedal ganglion (Fig. 5), each consisting of about 20-25 small (15-30 μm) neurons displaying immunoreactivity in a part of the cytoplasm (Fig. 1H).

3.1.2 K_v3.4 channel immunoreactive neurons

K_v3.4-immunoreactive (IR) neurons and fibers were present everywhere the *Helix* CNS (Fig. 5). In the ventro-medial part of the paired buccal ganglia, medium size (50-60 μm) labeled neurons were located (Fig. 3A). The labeled neurons sent thick axons to the buccal neuropil which after branching entered the buccal commissure (Fig. 3A). In the neuropil labeled varicose processes were found juxtaposed the labeled thick axons suggesting a close contact with them (Figs. 3B, C). In addition, medially and laterally located clusters of small (10-15 μm) size neurons, which could be observed throughout the ganglion from the dorsal to the ventral surface, also displayed positive immunoreaction (Fig. 3B). At high magnification immersion oil view both the medium and small diameter cells contained dot-like immunoprecipitation located close to the cell membrane, in addition to the usual diffuse cytoplasmic appearance (Fig. 3D, E). One of the identified giant motoneurons, the B2 cell (Altrup et al. 1982) also displayed immunolabeling (Fig. 5). In the cerebral ganglion groups of labeled cells consisting of 8-10 (5-8 μm) in the PC and 25-40 (20-30 μm) neurons in the metacerebrum could be found (Figs. 3 F, G, 5). The K_v3.4-IR neurons visualized in the pedal lobe projected with their axons to the cerebro-pedal connective (Fig. 3F). In the rest of the CNS, the subesophageal ganglion complex, additional small groups of K_v4.3 labeled neurons

were present (Fig. 5), except a large cluster (30-40) of labeled cells in the cerebro-pedal lobe of the pedal ganglion (Fig. 3H). All over the neuropil branching varicose axons was observed.

3.1.3 K_v4.3 channel immunoreactive neurons

The presence of K_v4.3 immunolabeled elements was also notable in the whole CNS except the visceral ganglion where they were absent (Figs. 4, 5). In addition to several labeled neuronal groups and fibers in the neuropil, labeled elements in non-neuronal tissues in the vicinity of the ganglia could also be observed. In the buccal ganglion a large cell cluster containing about 30-40 cells was found, which extended through the whole ganglion from the dorsal to the ventral surface (Fig. 4A). In the PC, K_v4.3-IR globuli cells were partly located along the borderline between the medullary (terminal) neuropil and the cell body layer (Fig. 4B). Their number was small and the strong immunolabeling dominated the entire cytoplasm. In the cell body layer septal axon bundles formed extensive branching which originated at least partly from groups of labeled cell bodies located at the lateral surface of the PC (Fig. 4C, D). The terminal neuropil showed a slight overall staining, in contrast to the internal mass characterized by an intensive immunoreaction. The subesophageal ganglion complex contained several K_v4.3-IR cell groups, most of them occurred in the pedal and pleural ganglia, while the visceral ganglion was free of labeled neurons (Figs. 4E, F, 5). A remarkable large group of K_v4.3-IR neurons located in the caudo-medial lobe of the pedal ganglion (Fig. 4C). Their average size was 25-30 μm and they projected with their thick axons to the neuropil ending up there often with arborization. In the pleural ganglion large K_v4.3-IR cell groups consisting of at least 50-60 neurons of 25 μm diameter were present, surrounding almost the entire neuropil area (Fig. 4F). Towards the periphery in the pallial nerve roots originating from the right parietal ganglion fine K_v4.3-IR varicose fibers were running among unlabeled cell bodies while other labeled axons projected parallel inside the nerves (Fig. 4E).

Only in case of K_v4.3 channel, immunolabeled fibers were also found outside but near to the CNS: extensive branchings were present in the connective tissue sheath surrounding the ganglia (Fig. 4A) and the aorta wall was also innervated by K_v4.3-IR processes (Fig. 4H).

At ultrastructural level we have found HRP-DAB labeled K_v4.3-IR varicosities containing 80-100 nm granular vesicles in the neuropil of the procerebrum and in the neuropil region of other, for example the pedal ganglia of the CNS (Fig. 6). The labeled profiles were typical small diameter varicosities in the procerebrum (Figs. 6A, B), meanwhile in the pedal ganglion large (3-4 μm) axon profiles completely filled with granular vesicles were also found (Fig. 6C). The quality of immunolabeling was different, displaying sometimes typical strongly electron dense precipitations distributed overall in the axon profiles (Figs. 6A, B) and sometimes being present as fine appositions partly attached to the axon membranes and the granular vesicles, and partly distributed in the axoplasm (Fig. 6C), lending a general appearance of increased electron density to the labeled profiles emerging from the surroundings or being distinguished from unlabeled axon profiles (Figs. 6A, C).

3.2 Immunodetection of K_v2.1, K_v3.4 and K_v4.3 channel peptides

The immunodetection of anti-K_v2.1, anti-K_v3.4 and anti-K_v4.3 antibodies was tested applying Western blot. In case of K_v2.1 channel, a prominent band was observed at the expected molecular weight, about 110 kDa, for both the CNS and in the PC (Fig. 7). Both in the labeled CNS and the PC immunoreactive band were clearly seen. In case of K_v3.4 channel the specific band, which was totally blocked in the pre-absorption control experiment, appeared at 250 kDa in the CNS (Fig. 7), which is the double weight as described in the literature (Wang et al., 2004). In the PC just a very slightly band could be seen and it correlates well with the tissue IHC results, where the labeled cells were small in number. In

case of K_v4.3 channel we have investigated both the total and the desheathed CNS, and the PC and the connective tissue sheath alone. The blotting experiments demonstrated a band which corresponded to a 73 kDa weight protein in each case. The presence of the specific band in the isolated connective tissue sheath preparation supports our immunohistochemical observation on the strong innervation of the sheath by K_v4.3-IR fibers. The secondary bands on the membrane strips in case of all K^+-channels were maybe the result of protein degradation processes. In a preabsorption control test when blocking the antibody with its peptide, the specific band disappeared in case of K_v4.3 and only the secondary band remained.

3.3 Electrophysiological properties of K^+-channels containing neurons

When the membrane potential of the B2 neuron located in the buccal ganglion and expressing K_v3.4 channel immunoreactivity was stepped above -50 mV after the hyperpolarizing prepulse to -100 mV for 200 ms a typical fast transient K-current (A-current) was activated, and inactivated in a solution in which NaCl was omitted and 5mM TEA was added to depress inward Na-, delayed rectifier and Ca-activated K-currents (Fig. 8A). Current traces shown in Fig. 8A were obtained subtracting currents without hyperpolarizing prepulse to -100 mV from those obtained from prepulse experiment. Kinetic parameters of A-currents were similar to other neuronal A-type currents recorded from both vertebrate and invertebrate neurons: they rose rapidly to a peak value and decayed exponentially during the 400 ms depolarizing pulse (Rudy, 1988). The A-type current was more sensitive to 4-AP (Fig. 9B) than to TEA and could be blocked by 100 nM of BDS-II, the specific blocker of K_v3.4 channel (Fig. 8A'). The recovery after BDS-II block was complete (Fig. 9A).

Using the same voltage-protocol and the same physiological saline, quite different transient K-current was recorded from neurons located in the caudo-medial lobe of the pedal

ganglion and expressing K_v4.3 immunoreactivity channels (Fig. 8B). These A-type currents were smaller in amplitude and also slower in their kinetics however the voltage-dependence was much similar to that of the fast transient A-current, although the currents could also be activated without hyperpolarizing prepulse (Fig. 8B'). The current could also be blocked by 4-AP, however, it was less sensitive to TEA. The slow A-type transient currents were expressed in the neurons of pedal ganglion and resembled to currents described in *Aplysia* by Furukawa et al. (Furukawa et al., 1992), although the channel type was not identified by these authors.

Typical delayed K-current recordings from PC neurons expressing K_v2.1 channel immunoreactivity are shown in Fig. 8C. Currents recorded in Na-free physiological solution started to be activated after a short delay and after reaching the steady state level they were maintained for the duration of the depolarizing pulse. The current-voltage relationship shows that the currents were activated from -20 mV from the HP=-60 mV, where the A-currents are almost completely inactivated. Currents through delayed rectifier channels were sensitive to block of 20 mM TEA and relative insensitive to blocking by 4 mM 4-AP and apamine (not shown) (Fig. 9B). The block by TEA was concentration dependent and reversible. The contribution of the Ca-dependent K-current (Crest et al., 1999) was tested with apamine (not shown). It was found negligible since 10^{-6} M apamine decreased the A-current amplitude less than 5%. The current recorded from the snail neurons expressing K_v2.1 channels is similar to the vertebrate delayed rectifier K-current recorded from neurons expressing K_v2.1 type channels (Kristen et al., 2010).

4. Discussion

4.1 K^+-channels in the *Helix* CNS

It has been known for a long time that in the nervous system of mollusks there are a number of vertebrate-like peptide materials and some of them possess the same amino acid

sequence as the endogenous compound identified in vertebrates (Walker, 1986). This important finding suggested that a part of the signal molecules might have developed from common precursors, a characteristic evolutionary feature which they share with monoamine and amino acid transmitters (see. e.g. Venter et al., 1988; Barreiro-Iglesias et al., 2010). Going further on this way, receptors and related molecules such as ion channels involved in signaling processes at the membrane level may also have a common in structural/molecular organization, including basic amino acid sequence. Therefore it is not surprising that some of the very conserved and ancient voltage-dependent K^+-channels (Rudy, 1988; Lu et al., 2001; Yifrach, 2004) could be demonstrated in the *Helix* nervous system. Our immunohistochemical results provide a clear evidence for the distinct cellular localization of the different K^+-channels (K_v2.1, K_v3.4, K_v4.3) in the *Helix* CNS, suggesting their involvement in a number of intercellular connections. The Western blot analysis for K_v2.1 channel revealed bands indicative of 110 kDa, and K_v4.3 channel at 73 kDa weight proteins which are identical with the reactions obtained in mammals (Mohapatra et al., 2008; Yang et al., 2001), referring to the identity of the K^+-channels occurring in the gastropod CNS with those described in vertebrates. The double molecular weight of the K_v3.4 channel found in Western blot, which was completely blocked with the sequence specific control peptide, is probably due to the insufficient reductive effects during the antigen retrieval procedure. Anholt et al. (1980) have found that nicotinic acetylcholine receptors in the electric organ of *Torpedo californica* are equally active after reconstitution in model membranes both in monomer and dimer forms, and the internal modification (e.g. disruption of the disulfide bridge between subunits) did not affect the induced cation flux response or desensitization. Therefore, receptor dimerization may indicate a structural but not a functional change. K^+-channels also consist of subunits and in vertebrates the native channel structure is a homomultimer. There are evidences that co-expression of two kinetically or pharmacologically distinct K^+-channels results in a hybrid

behavior of ionic currents (Christie et al., 1990; McCormack et al., 1990). It indicates that heteromultimeric channels possibly contribute to the channel functional diversity. The fact that BDS-II blocking was effective during voltage-clamp recording confirms the existence of the $K_v3.4$ channel in *Helix* CNS. We presume that the dimer form of the $K_v3.4$ channel in *Helix* may represent a species-specific structural modification rather than a functionally important universal feature. Voltage-clamp recording from neurons displaying immunoreactivity to the different K^+-channels proved the functional existence of the channels in the *Helix* CNS. So our results provide further evidence for the diversity of cell signaling pathways in the gastropod nervous system. The selective distribution of the different K^+-channels studied may contribute to shaping the functioning of nerve cells in intercellular communication. Namely, the antibodies used labeled distinct sets of neurons, meanwhile innervating by their processes the neuropil of the ganglia of the CNS. The overall discrete number of labeled cell groups, representing subpopulations of larger units of neurons, suggests a well-defined specific role for the K^+-channels studied. The immunohistochemical analysis of three Na^+-channels, $Na_v1.9$, $Na_v1.8$, and $Na_v1.7$, in the *Helix* CNS also revealed a kind of differential presence of the cell groups labeled by the antibodies raised against the channels (Kiss et al., 2012). It strengthens our suggestion that the cell groups containing the different ion channels are involved in different regulatory processes. On the other hand, the rich axon arborization observed in the neuropils throughout the CNS refers to an extensive involvement in synaptic (and non-synaptic) events. An additional role of K^+-channels in signaling processes is indicated by the observation that $K_v4.3$ immunoreactivity occurred in the neural sheath and the aorta wall. The labeling was clearly bound to varicose fibers possibly innervating the muscle fibers present in both tissues. Earlier studies showed that the connective tissue sheath of *Helix* was innervated by 5-HT-IR and FMRFamide-IR elements (Hernádi et al 1989; Elekes and Nässel 1990; Elekes 1991), and that 5-HT-IR varicosities

formed unspecialized close membrane contacts with muscle fibers in the ganglionic connective tissue sheath (Elekes, 1991). The localization of the labeled fibers in the aorta wall far from the lumen (Fig. 1D) can also be interpreted that they innervate the aorta wall musculature. This form of innervation resembles that of the axon network supplying the muscle fibers in the wall of the salivary gland duct which is also comprised of an innermost epithelial cell layer along the lumen and an outer muscle layer (Elekes, 2000; Kiss et al., 2003, 2010). The complex regulation and transmitter background of the contractility of the muscular aorta wall have been previously described in *Aplysia* (see e.g. Sawada et al., 1981a, b; 1982; Sasaki et al., 2002).

4.2 Subcellular localization of K^+-channels in the *Helix* CNS

The localization and distribution of the HRP-DAB reaction product throughout the entire domain of the labeled neurons that is from cell body to the axon varicosities, refers to an "overall" role of the three K^+-channels studied in the different anatomical regions of *Helix* nerve cells. It involves the possibility that K^+-channels play a role in both axo-axonic and axo-somatic signaling in the *Helix* CNS, hence acting in both pre- and postsynaptic processes. The labeling of neuronal perikarya throughout in the CNS raises two possibilities. It may indicate the site of the synthesis of the channels but also their involvement in axo-somatic contacts. Axo-somatic contacts were visualized in the gastropod (*Aplysia, Helix*) nervous system (Schwartz and Shkolnik, 1981; Elekes et al., 1985; Elekes, 1991), including the globuli cell bodies in the PC of *Helix* and *Limax* (Elekes et al., 2013). Interestingly, however, no $K_v2.1$-IR varicosities could be observed over $K_v2.1$-IR globuli cell bodies, indicating the role of this channel type elsewhere in the PC then on the $K_v2.1$ containing neurons themselves.

We also have analyzed the localization of one of the three K^+-channels, $K_v4.3$, at ultrastructural level following HRP-DAB reaction. It was found that the labeled varicosities were characterized by a rather uniform fine structure, containing one type of large granular vesicles (80-100 nm), meanwhile in the vicinity one could find other unlabeled elements containing either smaller (50-60 nm) granular vesicles or large size (120-160 nm) granules of irregular form and variable electron density. According to our opinion, the situation parallels with our light microscopic observation, according to which the anti-K^+-channel antibodies used do not label the neuronal elements throughout the CNS as a functionally general component of the nerve cell membrane. In contrary, the selective labeling of a single axon profile type supports the view that the different K^+-channel family members may function in different nerve cell populations, hence being involved in different intercellular regulatory processes.

4.3 Comparison of the distribution of the nerve cells containing different K^+-channels

Compared the distribution of the nerve cells containing the different K^+-channels both overlapping and certain differences can be established (Fig. 5). In the cerebral ganglion, most of the labeled cell groups share a similar anatomical localization, but those in the PC. In the PC the same type of small (5-8 μm) globuli cells was labeled with the different anti-K^+-channel antibodies, forming however mostly smaller units in different regions of the cell body layer. At the same time, the larger (12-15 μm) globuli cells localized along the outer marginal surface of the PC displayed no immunoreactivity against any of the antibodies applied. In a recent study analyzing the distribution of Na^+-channels, large units of globuli cells immunoreactive to $Na_v1.9$ and $Na_v1.8$ antibodies, respectively, have been demonstrated in the PC, among which a number of labeled neurons of larger diameter were also observed (Kiss et al., 2012). It means that the seemingly uniform population of globuli cells do definitely may

function with different sets of K^+- and Na^+-channels. We suggest that the larger size bursting neurons representing only about 10% of the total globuli cell population (see Chase 2002; Nikitin et al., 2005) do possess K^+-channels different from the three ones investigated in the present study, meanwhile the non-bursting cells forming the bulk of the globuli cell population may function, at least partly, with a variable sets of Na^+- and K^+-channels identified in the present and our recent studies (Kiss et al., 2012; Pirger et al, 2013). The buccal ganglia, where the feeding network is located of the gastropod CNS (Chase, 2002), smaller and larger cell clusters were found labeled for the K^+-channels. The labeled nerve cells occurred in different regions or if in the same one, which was the case of the caudal region of the cell body layer near the esophageal and salivary nerve roots, the size of the labeled cells was different (15-20 um vs 30-40 um cell body diameters). These ganglia are also the site of a number of identified giant neurons (Altrup and Speckmann, 1992). One of them, the B2 cell displayed immunopositivity in our experiments following the application of antibodies raised against both $K_v3.4$ and $K_v4.3$ channels. B2 functions with acetylcholine and innervates the salivary gland (Altrup and Speckmann, 1992). Interestingly, other physiologically identified giant neurons such as e.g. the cerebral serotonergic (CGC) neuron, the FMRFamide containing (C3) cell or the pedal dopaminergic RPeD1 cell (Pentreath et al., 1982, Cottrell et al., 1983; see also Chase, 2002) remained unlabeled when applying any of the three channel antibodies. We assume that they express (and function with) other member(s) of the K^+-channels, referring to the possibly differential distribution and role of the of K^+-channel family members in the *Helix* (and other snail) CNS. In the subesophageal ganglion complex partial overlapping could be seen only in the pleural and pedal ganglia, where groups of $K_v2.1$-IR, $K_v3.4$ and $K_v4.3$-IR cells occurred in the rostro-medial and rostro-lateral lobes of the pedal ganglion and around the origin of the cerebro-pedal and cerebro-pleural connectives, respectively. To sum up, this kind of localization may indicate, on the

one hand, that selective sets of K^+-channel containing neurons are involved in different regulatory systems within the same groups of neurons. On the other hand, the localization of the three K^+-channels in clearly different cell groups, as for example in the PC, the viscero-parietal ganglia and the caudo-medial lobe of the pedal ganglion shows that there are also cell groups containing only one out of the three channels studied which suggests that they are involved in a single intercellular regulatory process.

5. Conclusions

In summary, our results provided data on the distribution and for the possible role of three different K^+-channels in the CNS of the snail, *Helix pomatia*. The distribution of the K^+-channels studied in the different ganglia possibly refers to their functional diversification involved in different intercellular signaling. We have also demonstrated the presence of a K^+-channel ($K_v4.3$) in the periphery, suggesting its role in neuromuscular events. Voltage clamp experiments revealed the functional existence of the different K^+-channels in cell types previously demonstrated to be immunoreactive to one of antibodies raised against them, hence proving the functional presence of these membrane compartments in the soma of *Helix* central neurons. The ultrastructural demonstration of the selective labeling of one type of varicosities by anti-$K_v4.3$ antibody supports the view that the different K^+-channels may occur in different population of neurons. Our results provide also a steady basis for future experiments aiming at the high resolution identification of membrane compartmentalization of these potassium channels in the *Helix* nervous system. To reveal the exact subcellular localization of the ion channels may help define further details and essential aspects of processes of intercellular connections and neuronal functions underlying different behaviors. On the other hand, the current findings contribute to resolve and identify the role of different molecular components

of interactions at synaptic and non-synaptic membrane levels. Finally, our results also provide a basis for a better insight in the diversity of cell signaling pathway(s) in the gastropod CNS.

6. Acknowledgements

The skillful technical assistance of Mrs. Zsuzsanna N. Fekete and Mr. Boldizsár Balázs is greatly appreciated. The contribution of Dr. Zoltán Nusser (Institute of Experimental Medicine, HAS, Budapest) to the work by donating antibodies in an initial phase of the experiments is also acknowledged. Z. S. was supported by the János Bolyai Research Scholarship of the Hungarian Academy of Sciences. This work was supported by an OTKA grant, No. 78224 to K. E.

7. References

Alkon, DL, Sakakibara M, Forman R, Harrigan J, Lederhendler I, Farley J (1985), Reduction of two voltage-dependent K^+ currents mediates retention of a learned association. Behav Neural Biol 44:278-300.

Altrup U, Speckmann EJ (1982), Responses of identified neurons B1, B2 and B3 in the buccal ganglia of *Helix pomatia* to stimulation of ganglionic nerves. Comp Biochem Physiol A 72: 643-657.

Altrup U, Speckmann EJ (1994), Identified neuronal individuals in the buccal ganglia of *Helix pomatia*. Neurosci Behav Physiol 42:1090-115.

Anholt R, Lindstrom J, Montal M (1980), Functional equivalence of monomeric and dimeric forms of purified acetylcholine receptors from *Torpedo californica* in reconstituted Lipid Vesicles. Eur J Biochem 109:481 -487.

Azanza MJ, Pérez-Castejón C, Pes N, Pérez-Bruzón RN, Aisa J, Junquera C, Maestú C, Lahoz M, Martínez-Ciriano C, Vera-Gil A, Del Moral A (2008), Characterization by immunocytochemistry of ionic channels in *Helix aspersa* suboesophageal brain ganglia neurons. Histol Histopathol 23:397-406.

Barreiro-Iglesias A, Laramore C, Shifman MI, Anado´n R, Selzer ME, Rodicio MC (2010), The sea lamprey tyrosine hydroxylase: cDNA cloning and in situ hybridization study in the brain. Neuroscience 168:659–669.

Battonyai I, Serfőző Z, Elekes K (2012), Potassium channels in the *Helix* central nervous system: preliminary immunhistochemical studies. Acta Biol Hung 63 (Suppl. 2)146-150.

Baxter DA, Byrne JH (1990), Differential effects of cAMP and serotonin on membrane current, action-potential duration, and excitability in somata of pleural sensory neurons of *Aplysia*. J Neurophysiol 64:978-990.

Birnbaum SG, Varga AW, Yuan LL, Anderson AE, Sweatt JD, Schrader LA (2004), Structure and function of Kv4-family transient potassium channels. Physiol Rev 84:803-33.

Butler A, Wei A, Baker K, Salkoff L (1989), A family of putative potassium channel genes in Drosophila. Science 243:943-947.

Choe S (2002), Potassium channel structures**.** Nat Rev Neurosci 3:115-21.

Chase R (2002), Behavior and its neural control in gastropod molluscs. Oxford University Press, Oxford-New York.

Christie MJ, North RA, Osborne PB, Doulgass J, Andelman JP (1990), Heteropolymeric potassium channels expressed in *Xenopus* oocytes from cloned subunits. Neuron 4:405.

Collin C, Ikeno H, Harrigan JF, Lederhendler I, Alkon DL (1988), Sequential modification of membrane currents with classical conditioning. Biophys J 54, 955-960.

Cottrell GA, Schot LP, Dockray GJ (1983), Identification and probable role of a single neuron containing the neuropeptide *Helix* FMRFamide. Nature 304:638-640.

Crest ME, Hile E, Pin T, Watanabe K, Gola M (1999), Plateau-generating nerve cells in *Helix*: properties of the repolarizing voltage-gated and Ca2+-activated potassium currents. J. Exp Biol 152, 211-241.

Edward C Conley and William J Brammar (1999), The ion channel FactsBook IV, Voltage-gated Channels. pp. 196-644. Academic Press, London.

Elekes K (1991), Serotonin-immunoreactive varicosities in the cell body layer and neural sheath of the snail, *Helix pomatia*, ganglia. An electron microscopic immunocytochemical study. Neuroscience 42:583-591.

Elekes K (2000), Ultrastructural aspects of peptidergic modulation in *Helix pomatia*. Microsc Res Tech 49:534-546.

Elekes K, Nässel DR (1990), Distribution of FMRFamide-like immunoreactive neurons in the central nervous system of the snail *Helix pomatia*. Cell Tissue Res 262:177-190.

Elekes K, S.-Rózsa K, Vehovszky Å, Hernádi L, Salánki J (1985), Ultrastructural organization of nerve cells and synaptic connections in the intestinal nerve of the snail *Helix pomatia* L. Cell Tissue Res 239:611-620.

Elekes K, Kiss T, Fujisawa Y, Hernádi L, Erdélyi L, Muneoka Y (2000), *Mytilus* inhibitory peptides (MIP) in the central and peripheral nervous system of the pulmonate gastropods

Lymnaea stagnalis and *Helix pomatia*: distribution and physiological actions. Cell Tissue Res 302:115-134.

Elekes K, Battonyai I, Kobayashi S, Ito E (2013), Organization of the procerebrum in terrestrial snails (*Helix, Limax*) revisited: cell mass layer synaptology and its serotonergic input system. Brain Struct Funct 218:477-490.

Frick A, Johnston D (2005), Plasticity of dendritic excitability. J Neurobiol 64:100-15.

Furukawa Y, Kandel ER, Pfaffinger PJ (1992), Three types of early potassium transient currents in *Aplysia* neurons. J Neurosci 12:9898-1000.

Gelperin A (1999), Oscillatory dynamics and information processing in olfactory systems. J Exp Biology 202: 1855-1864.

Hernádi L, Elekes K, S.-Rózsa K (1989), Distribution of serotonin-containing neurons in the central nervous system of the snail *Helix pomatia.* Cell Tissue Res 262:177-190.

Hille B (2001), Ion Channels of Excitable Membranes (3rd ed.). Sunderland, Mass: Sinauer Associates.

Hodgkin AL, Huxley AF (1952), A quantitative description of membrane current and its application to conduction and excitation in nerve. J Physiol (Lond) 117:500-544.

Kaang B.-K., Pfaffinger PJ, Grant SGN, Kandel ER, Furukawa Y (1992), Overexpression of an *Aplysia* Shaker K^+ channel gene modifies the electrical properties and synaptic efficacy of identified *Aplysia* neurons. Proc Natl Acad Sci USA 89:1133-1137.

Kandel, ER, Schwartz JH (1982), Molecular biology of learning: modulation of transmitter release. Science 218:433-443.

Kiss T, Hiripi L, Papp N, Elekes K (2003), Dopamine and serotonin receptors mediating contractions of the snail, *Helix pomatia*, salivary duct. Neuroscience 116:775-790.

Kiss T, Hernádi L, László Z, N. Fekete Zs, Elekes K (2010), Peptidergic modulation of serotonin and nerve elicited responses of the salivary duct musculature in the snail, *Helix pomatia*. Peptides 31:1007–1018.

Kiss T, László Z, Pirger Z (2012), Cellular localization and kinetic properties of $Na_v1.9$, $Na_v1.8$-, and $Na_v1.7$-like channel subtypes in *Helix pomatia*. Neuroscience 203, 78–90.

Kobayashi S, Hattori M, Elekes K, Ito E, Matsuo R (2010), FMRFamide regulates oscillatory activity of the olfactory center in the slug. Eur J Neurosci 32:1180-1192.

Kollo M, Holderith NB, Nusser Z (2006), Novel subcellular distribution pattern of A-type K+ channels on neuronal surface. J Neurosci 26:2684-91.

Kristen MS, O'Connell RL, Tamkun MM (2010), Localization-dependent activity of the Kv2.1 delayed-rectifier K^+ channel. Proc Natl Acad Sci U.S.A. 107:12351-12356.

Kues WA, Wunder F (1992), Heterogeneous Expression Patterns of Mammalian Potassium Channel Genes in Developing and Adult Rat Brain. Eur J Neurosci 4:1296-1308.

Kurachi Y, Jan LY, Lazdunski M (1999), Potassium Ion Channels: Molecular Structure, Function, and Disease. Current Topics in Membranes. Academic Press, New York.

Lu Z, Klem AM, Ramu Y. (2001), Ion conduction pore is conserved among potassium channels. Nature 413:809-813.

Magidovich E, Yifrach O (2004), Conserved gating hinge in ligand- and voltage-dependent K+ channels. Biochemistry 43:13242-71324.

Migliore M, Shepherd GM (2002), Emerging rules for the distributions of active dendritic conductances. Nat Rev Neurosci 3:362-70.

Mohapatra DP, Siino DF, Trimmer JS (2008), Interdomain cytoplasmic interactions govern the intracellular trafficking, gating, and modulation of the Kv2.1 channel. J Neurosci 28:4982-94.

Nikitin ES, Zakharov IS, Samarova EI, Kemenes G, Balaban PM (2005), Fine tuning of olfactory orientation behavious by the interaction of osciallatory and single neuronal activity. Learn Mem 7:422-432.

Pentreath W., Berry MS, Osborne NN (1982), The serotonergic cerebral cells in gastropods. In: Osborne N. N. (ed.) Biology of serotonergic transmission. Wiley, New York, pp. 457-513.

Pfaffinger PJ, Siegelbaum SA (1990), K^+ channel modulation by G proteins and second messengers. In: Potassium channels: structure, classification, function and therapeutic potential (Cook NS, ed), 117-153 Chicester: Norwood.

Pfaffinger PJ, Furukawa Y, Zhao B, Dugan D, Kandel ER (1991), Cloning and expression of an *Aplysia* K channel and comparison with native *Aplysia* K currents. J Neurosci 11:918-927.

Pirger Z, Battonyai I, Krajcs N, Elekes K, Kiss T (2013), Voltage-gated membrane currents in neurons involved in odor information processing in snail procerebrum. Brain Struc Funt DOI 10.1007/s00429-013-0526-6.

Rudy B (1988), Diversity and ubiquity of K-channels. Neuroscience 25:729-749.

Sasaki K, Fujisawa Y, Morishita F, Matsushima O, Furukawa Y (2002), The enterins inhibit the contractile activity of the anterior aorta of *Aplysia kurodai*. J Exp Biol 205:3525–3533.

Sawada M, Blankenship JE, McAdoo DJ (1981a), Neural control of a molluscan blood vessel, anterior aorta of *Aplysia*. J Neurophysiol 46:967-986.

Sawada M, McAdoo DJ, Blankenship JE, Price CH (1981b), Modulation of arterial muscle contraction in *Aplysia* by glycine and neuron. R14. Brain Res 207:486-490.

Sawada M, Hara N, Ichinose M, Maeno T (1982), Excitatory and inhibitory effects of acetylcholine on the anterior aorta muscle of *Aplysia*. J Neurosci Res 7:179-192.

Schwartz JH, Shkolnik LJ (1981), The giant serotonergic neuron of *Aplysia*: a multi-targeted nerve cell. J Neurosci 1:606-619.

Venter JC, Di Porzio U, Robinson DA, Shreeve SM, Lai J, Kerlavage AR, Fracek SP, Lentes K-U, Fraser CM (1988), Evolution of neurotransmitter receptor systems. Prog Neurobiol 30: 105-169.

Walker RJ (1986), Transmitters and modulators. The Mollusca vol 9, Neurobiology and behavior Part 2, pp. 279-453 Academic Press.

Walker RJ (1992), Neuroactive peptides with an RFamide or Famide carboxyl terminal. Comp Biochem Physiol 102C:213-222.

Walker RJ, Brooks HL, Holden-Dye L (1996), Evolution and overview of classical transmitter molecules and their receptors, Parasitology 113, S3-S33.

Wang L, Fyffe RE, Lu L (2004), Identification of a $K_v3.4$ channel in corneal epithelial cells. Invest Ophthalmol Vis Sci 45:1796-803.

Wei A, Jegla T, Salkoff L (1996), Eight potassium channel families revealed by the *C. elegans* genome project. Neuropharmacology 35, 805-829.

Wymore RS, Korenberg JR, Kinoshita KD, Aiyar J, Coyne C, Chen XN, Hustad CM, Copeland NG, Gutman GA, Jenkins NA, Chandy KG (1994), Genomic organization, nucleotide sequence, biophysical properties, and localization of the voltage-gated K+ channel gene KCNA4/Kv1.4 to mouse chromosome 2/human 11p14 and mapping of KCNC1/Kv3.1 to mouse 7/human 11p14.3-p15.2 and KCNA1/Kv1.1 to human 12p13. Genomics 20:191-202.

Yang EK, Alvira MR, Levitan ES, Takimoto KJ (2001), Kvbeta subunits increase expression of Kv4.3 channels by interacting with their C termini. Biol Chem 276:4839-44.

Yifrach O (2004), Hill coefficient for estimating the magnitude of cooperativity in gating transitions of voltage-dependent ion channels. Biophys J 87:822-830.

Legends

Fig. 1. $K_v2.1$ immunoreactive ($K_v2.1$-IR) elements shown in 16 µm cryostat sections in the *Helix* CNS. **A, B**: $K_v2.1$-IR neurons (arrows) clustered on the rostro-medial part of the dorsal surface of the right buccal ganglion. B2: unlabeled giant motoneuron. **C:** Labeled group of neurons (white arrow) in the globuli cell layer of the PC. Dotted black line indicates the borderline between the procerebral and the meta(post)cerebral neuropils. Note small bundle of labeled fibers (black arrowheads) and their varicose arborizations (black arrows) in the lateral part (pedal lobe) of the metacerebrum. **D**: Higher magnification view of the PC showing immunopositive globuli cells (white arrows). Insert: Labeled neurons displaying immunoreactivity concentrated in the thin layer of the cytoplasm (double arrow). **E**: Immunolabeled neurons (white arrows) and their varicose neurites (black arrows) in the lateral metacerebrum. **F**: Cluster of $K_v2.1$-IR cells (white arrow) located at the base of the mesocerebrum. **G**: Smaller (double arrow) and larger (white arrows) clusters of neurons displaying immunoreactivity in the right parietal ganglion. Black arrows indicate strong immunoreactivity at the origin of one of the right pallial nerves. **H**: Groups of $K_v2.1$-IR neurons (white arrows) in the anterior commissural lobe of the right pedal ganglion. Immunoreactivity located only in a part of their cytoplasm. gc: globuli cell layer, np: neuropil, mc: mesocerebrum, pcm: pedal comissure, rPa: right parietal ganglion. rPl: right pedal ganglion. Scale bars: A, B: 20 µm C:70 µm, D:30 µm, inset: 10 µm, E-H: 40 µm

Fig. 2. A: Camera lucida drawing based on three consecutive cryostat sections, showing the distribution of $K_v2.1$-IR cells (black symbols), axon processes (arrows) and bundles (open arrows) in the cerebral ganglion. Open symbols: unlabeled cells, dotted line (also in B): border between cell body layer and neuropil regions, PC: procerebrum, MtC: metacerebrum,

Me: mesocerebrum, cpdc: cerebro-pedal connective, cplc: cerebro-pleural connective. **B, C**: Enlarged details from the PC showing labeled (black symbols) and unlabeled (clear symbols) globuli cells in **B**, and the relationship of unlabeled cell bodies (open symbols) to $K_v2.1$ immunoreactive varicosities (small black dots) in **C**. Scale bars: A: 100 μm, B: 500 μm, C: 25 μm

Fig. 3. $K_v3.4$ immunoreactive elements in the *Helix* CNS. **A**: Dorsal surface of the paired buccal ganglia. In the ventro-medial part large (50-60 μm) neurons (stars) show immunoreactivity. Their thick axons are branching (encircled) in the neuropil (np) and then enter (arrow) the buccal commissure (bc). **B**: In a consecutive section to A small (10 μm) labeled neurons (arrows) and varicose axons (encircled) located over the large neurons (stars) can be seen. **C**: Higher magnification view of the varicose axons (arrows) in B, running over the large cells. **Inset:** Labeled varicosities (arrows) seen at high (immersion oil) magnification. **D, E**: Immersion oil view of the cytoplasmic localization of $K_v3.4$ immunoreactivity in medium (D) and small size (E) neurons in the buccal ganglion. $K_v3.4$ labeling appears as small dots (arrows). **F**: Detail of the postcerebrum of the cerebral ganglion. Labeled axons (long arrows) run long towards the pedal connectivum (cplc), originating from a labeled neuronal group (arrows) in the pedal lobe. Additional neurons (double arrows) display also immunoabeling in the pedal lobe. **G**: A small group of labeled neurons (arrows) in the procerebral globuli cell layer. **H**: In the cerebral lobe of the right pedal ganglion a large cluster of labeled cells (encircled) shows immunoreactivity. Close to them in the neuropil varicose axons are seen (arrows). Scale bars: A: 80 μm, B: 40 μm, C: 6 μm, inset: 1,2 μm. D: 7 μm, E: 8 μm F: 40 μm, G: 15 μm, H: 40 μm

Fig. 4. K_v4.3-IR elements in the CNS and periphery of *Helix*. **A**: Group of labeled neurons (encircled) on the dorsal surface of the right buccal ganglion. Note dense network of labeled fibers (arrows) in the connective tissue sheath. **B**: K_v4.3-IR neurons (arrows) lining up along the borderline between the neuropil (np) and globuli cell layer (gc) in the procerebrum. **C, D**: Immunolabeling in the procerebral lobe following HRP-DAB reaction. **C:** Sagittal section showing K_v4.3-IR septal axon branches (arrows) in the globuli cell layer (gc), originating at least partly from labeled globuli cells (double arrow). Note the overall slight staining in the terminal (np) and the intensive labeling of the internal (in) neuropil. **D:** Higher magnification of K_v4.3-IR septal axon branching (arrows). Double arrow: group of labeled globuli cells, long arrow: a solitary labeled neuron near the terminal neuropil (np). **E**: K_v4.3-IR neurons (double arrows) in the caudo-medial lobe of the pedal ganglia with their axons (arrows) projecting to the neuropil (np). **F**: Labeled cell clusters (arrows) around the neuropil area (np) in the right pleural ganglion. **G**: K_v4.3-IR fibers (arrows) running among unlabeled cells (asterisks) and parallel (double arrows) within one of the pallial nerve roots. **H**: The aorta wall is heavily innervated by K_v4.3-IR varicose axon processes (arrows). Scale bars: A: 18 μm, B: 18 μm, C, D, E: 35 μm, F: 30 μm, G: 30 μm, H: 30 μm

Fig. 5. Schematic mapping of the distribution of K_v2.1, K_v3.4 and K_v4.3-IR neurons (black symbols) in the *Helix* CNS. B2 and encircled (red) are the neurons used for the electrophysiological experiments. Estimated number of immunolabeled neurons: K_v2.1-IR neurons in cerebral ganglia (including procerebrum): 260, buccal ganglia: 80, subesophageal ganglion complex (including pedal ganglia, SOG): 300. K_v3.4-IR neurons in cerebral ganglia: 120, buccal ganglia: 60, SOG: 240. K_v4.3-IR neurons in cerebral ganglia: 320, buccal ganglia: 80, SOG: 300. Nerves: 1 esophageal; 2 salivary; 3, 4, 6 pharyngeal; 5 cerebro-buccal connective; 7 buccal commissure; 8 cerebro-pleural connective; 9 cerebro-pedal connective;

10 outer lip; 11 median lip; 12 inner lip; 13 optic; 14 olfactory; 15 internal peritentacular; 16: cerebral commissure; 17:left parietal; 18 anal; 19 intestinal; 20 right pallial nerves; 21 cutaneous; 22 pedal nerves; 23 anterior pedal commissure.

Fig. 6. Ultrastructure of K_v4.3-IR elements visualized by HRP-DAB reaction in the procerebrum (A, B), and in the pedal ganglion (C, D). **A, B** - Small size labeled varicosities (T) contain large (80-100 nm) granular vesicles (arrows) of different number in the procerebrum. Note an unlabeled profile (T1) near the labeled element in picture A, which contains granular vesicles of smaller size. A: unlabeled axons. **C** - A large labeled varicosity (T) in the pedal ganglion is densely packed with large granular vesicles. **D** - An unlabeled axon profile filled with granules of variable electron density, the morphology and size (120-160 nm) of which differs completely from those seen in the labeled profile in C. m= mitochondrium Scale bars: A, B: 0.5 μm, C, D: 0.25 μm

Fig. 7. Detection of K_v2.1, K_v3.4 and K_v4.3 antibody by Western blot. Lanes 1, 2: K_v2.1-IR bands in the CNS and PC. Black arrow: 110 kDa K_v2.1–IR bands. Lanes 3, 4: K_v2.1 antibody blocking with preabsorption peptide. Lanes 5, 6: K_v3.4-IR bands in the CNS and PC. Black arrow: 240 kDa K_v3.4–IR band in the CNS. The weak signal in the PC corresponds with tissue IHC data. Lanes 7,8: K_v3.4 antibody blocking with preabsorption peptide. 9-14: K_v4.3 antibody Western blots. 9, 10: CNS and connective tissue sheath (CT). 11, 12: CNS and procerebrum (PC). Black arrows: K_v4.3-IR bands at 73 kDa in the CNS, CT and PC. Red arrows: secondary bands. Lanes 13, 14: Preabsorption controls, red arrow shows the remained secondary band. Left side: molecular ladder, in kDa. Chemiluminescence method: lanes 1-10, HRP-DAB reaction: lanes 11-14.

Fig. 8. Three types of K^+-currents were recorded from different neurons of the snail CNS, showing immunolabeling against $K_v3.4$, $K_v4.3$ and $K_v2.1$ antibodies, respectively. A: Fast (A-type) transient outward current recorded from a $K_v3.4$-IR B2 giant cell located in the buccal ganglia (Fig. 5). The current traces were evoked by 600 ms depolarizing steps between -30 mV to +40 mV from a holding potential (HP) of -50 mV. Depolarization was preceded by a 200 ms hyperpolarization to -100 mV. Voltage-traces above current traces were recorded simultaneously throughout the voltage-clamp experiments. The rectangular shape of the voltage drop of the cell membrane potential reveals the stability of the clamp. A': Average current-voltage (I-V) relationship of recordings from six B2 neurons. The upper curve shows the average peak amplitudes recorded in snail physiological saline. The lower curve reveals the values obtained in the presence of 100 nM BDS-II, the specific blocker of $K_v3.4$ channel. B: Slow transient outward current from a neuron located in the caudo-medial lobe of pedal ganglion displaying $K_v4.3$-immunoreactivity (see Fig 4E, 5), evoked by depolarization steps from -60 mV to +10 mV. The HP was -60 mV. B': I-V characteristic shows that the activation threshold was similar to the current recorded from a caudo-medial pedal neuron expressing $K_v3.4$. C: Delayed outward currents of a procerebral neuron expressing $K_v2.1$ immunoreactivity (Figs. 1D, 5), induced by test potentials between 0 mV to + 60 mV starting from a HP of -60 mV. C': I-V relationship obtained from the averaged data of four PC cells. The delayed current activated at -20 mV.

Fig. 9. Blocking effect of 100 nM BDS-II, 20 mM TEA (A) and 4 mM 4-AP (B) on the amplitude of the transient outward current recorded from a B2 neuron. Blockers were applied at the time marked by arrows at the 5th episode and the wash out started at the 33rd episode. 4-AP was applied at the 5th episode and the wash out started at the 22nd episode. In both cases the recovery was almost complete. The time between the 100 mV depolarizing pulses

from the holding potential of -60mV was 30 sec. The test pulse was preceeded by hyperpolarizing prepulse to -100 mV. The inserts shows current traces obtained before and after 100 nM BDS II and 4 mM 4-AP exposure.

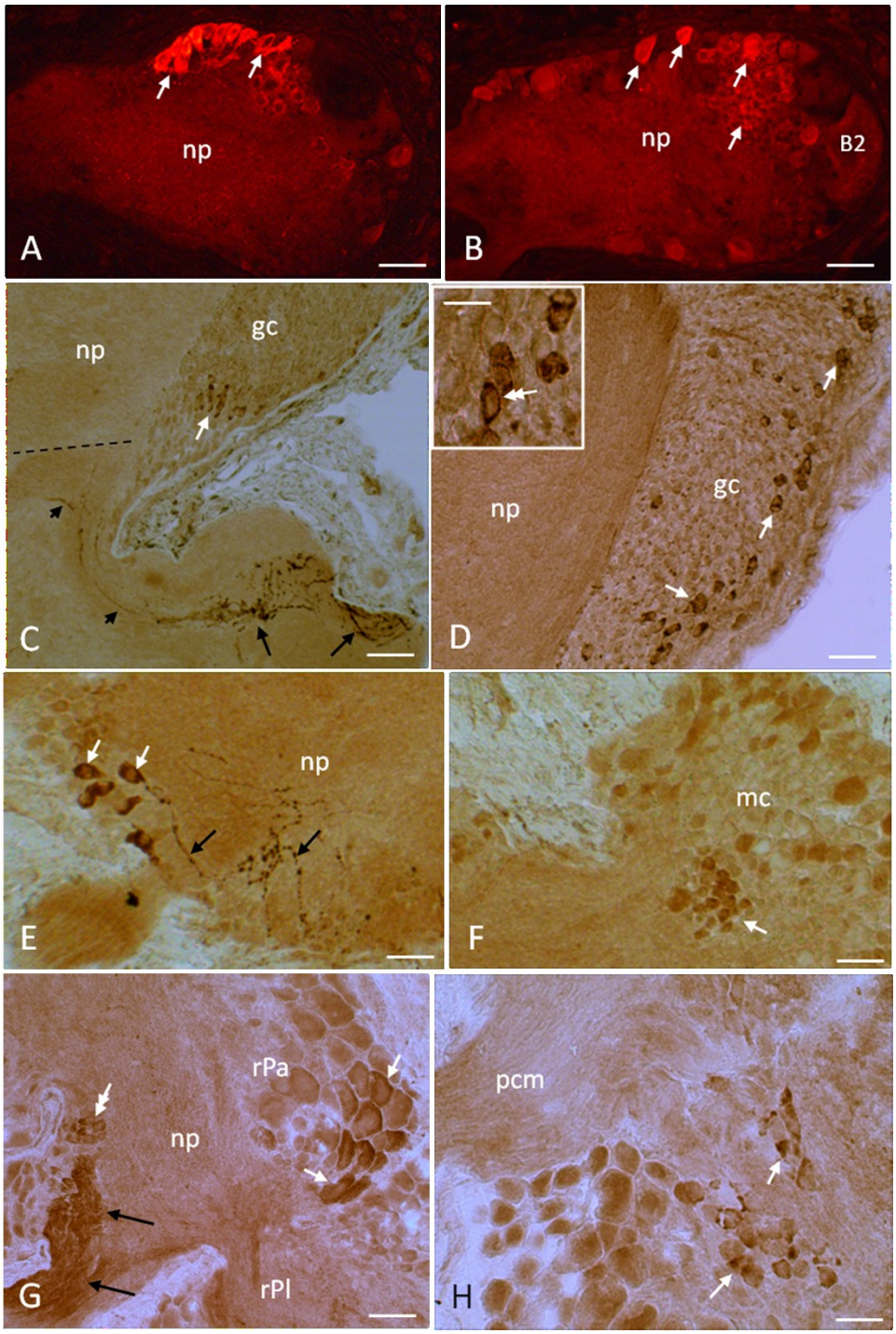

Fig.1

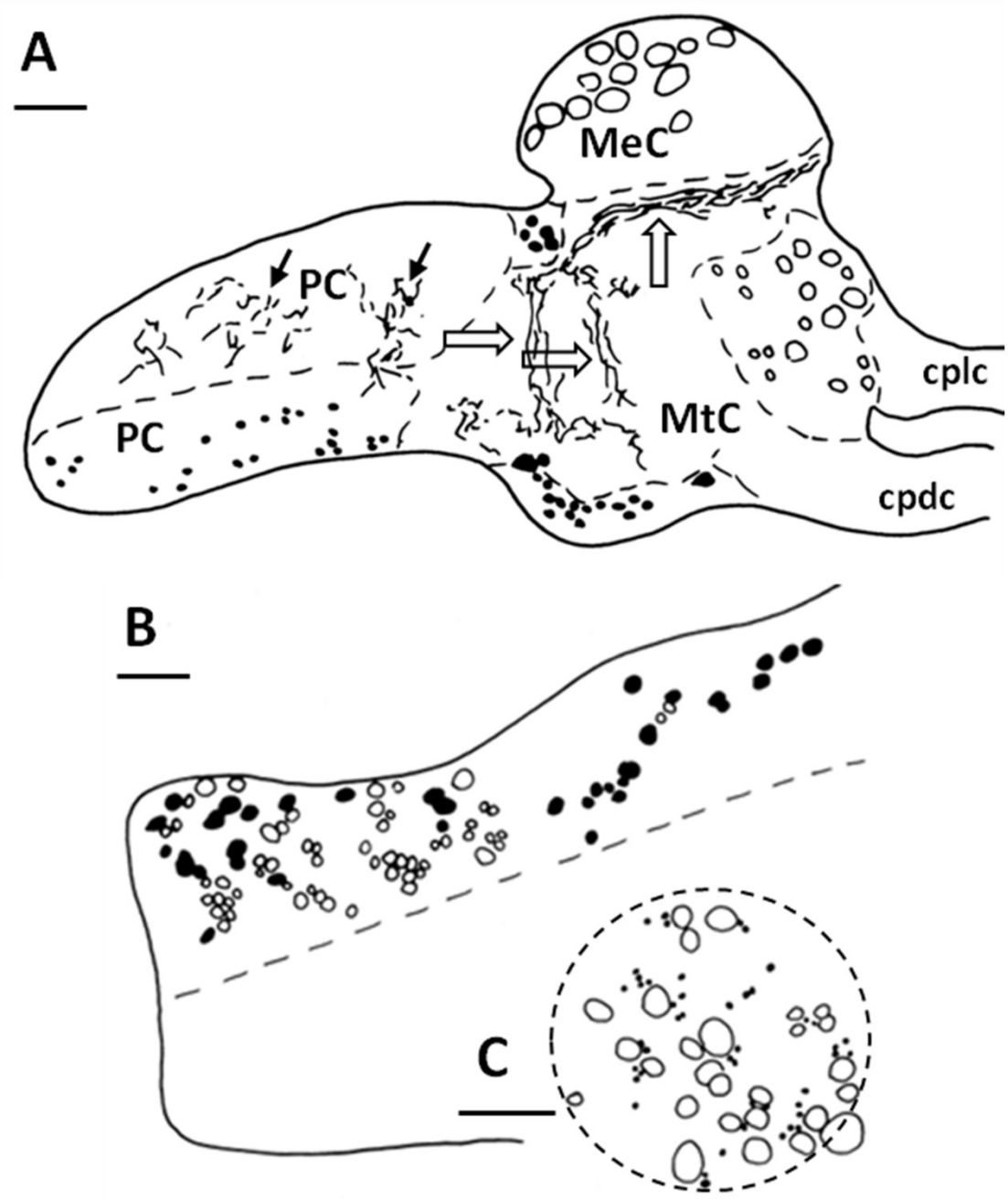

Fig. 2

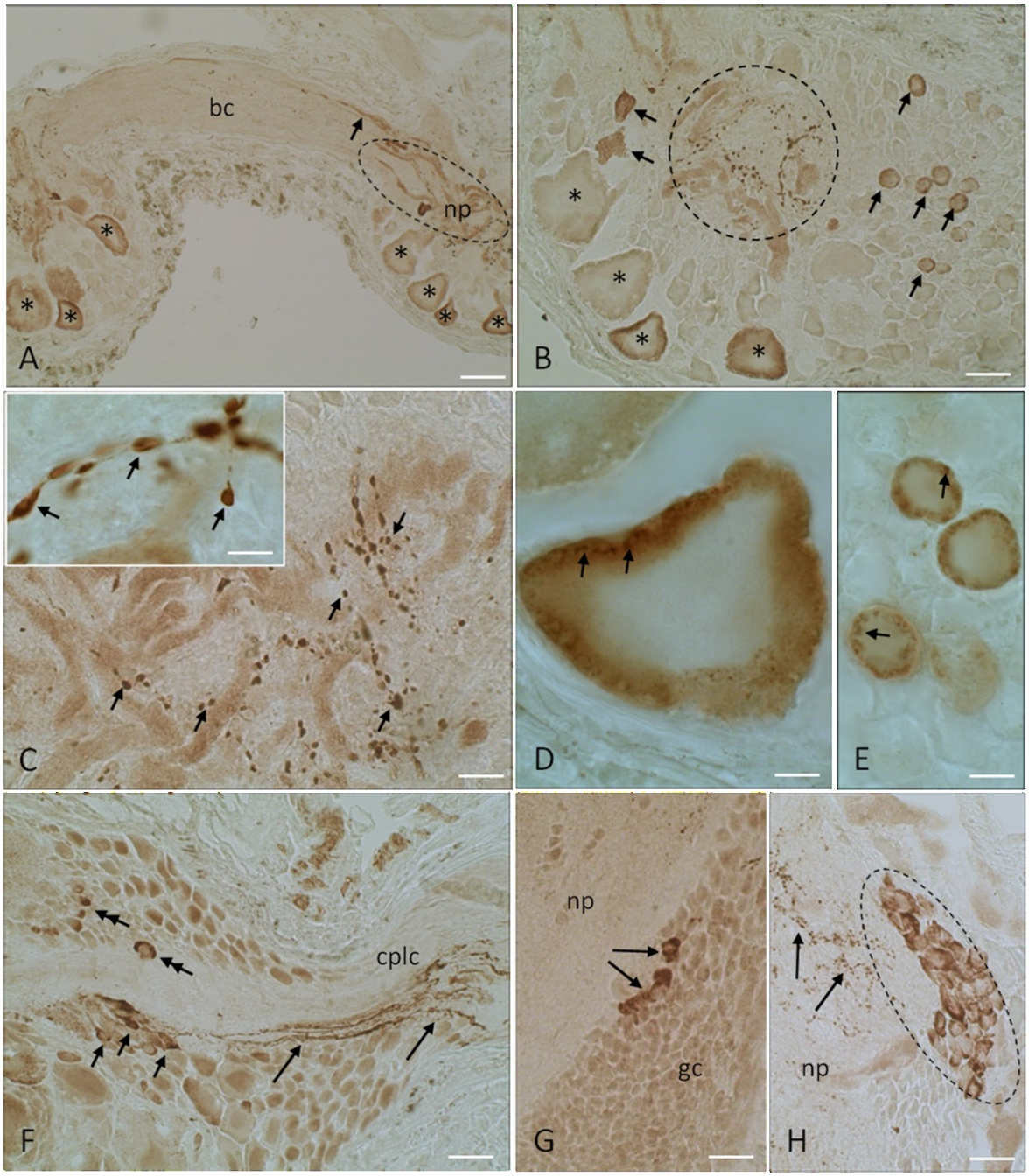

Fig. 3

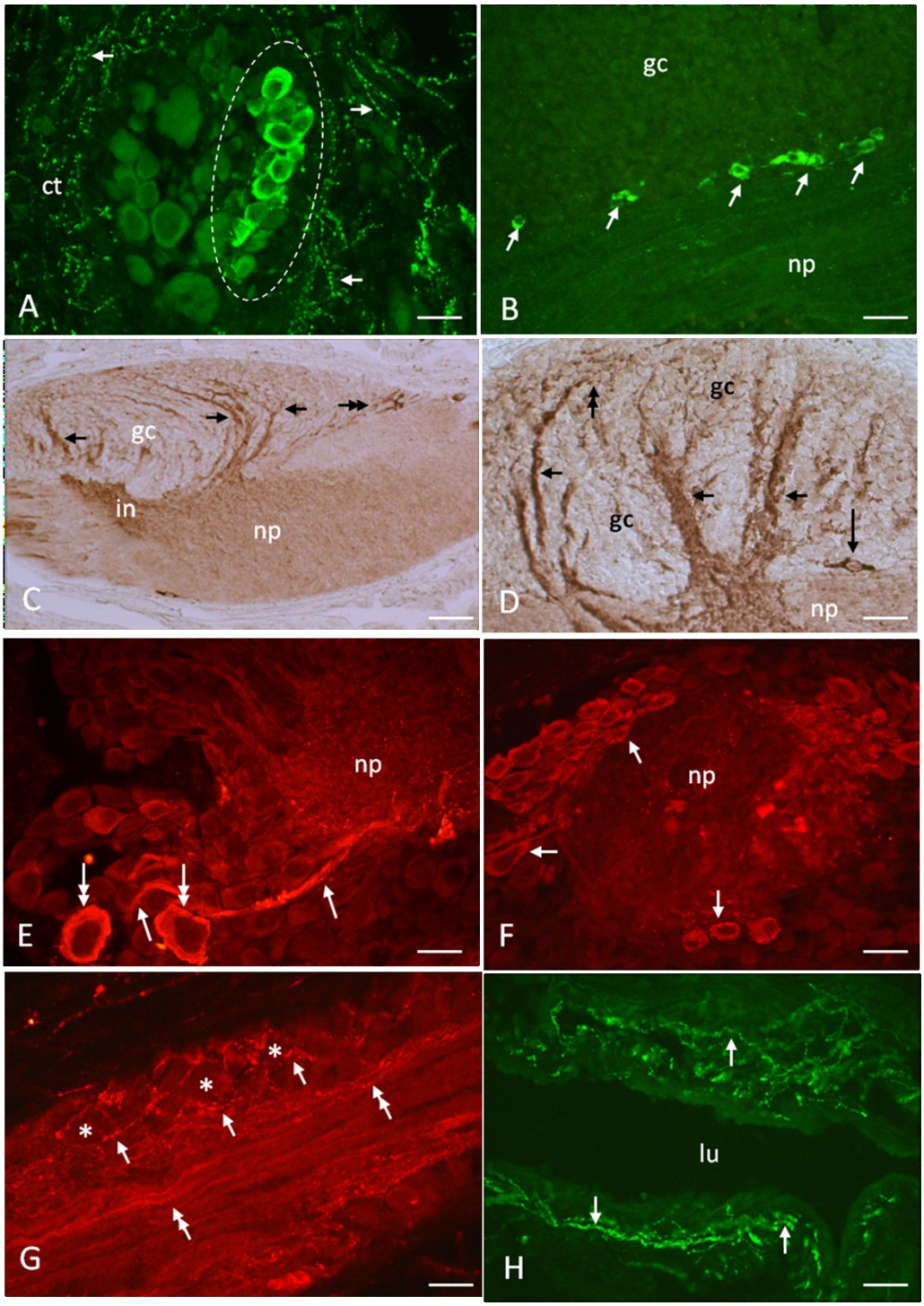

Fig. 4

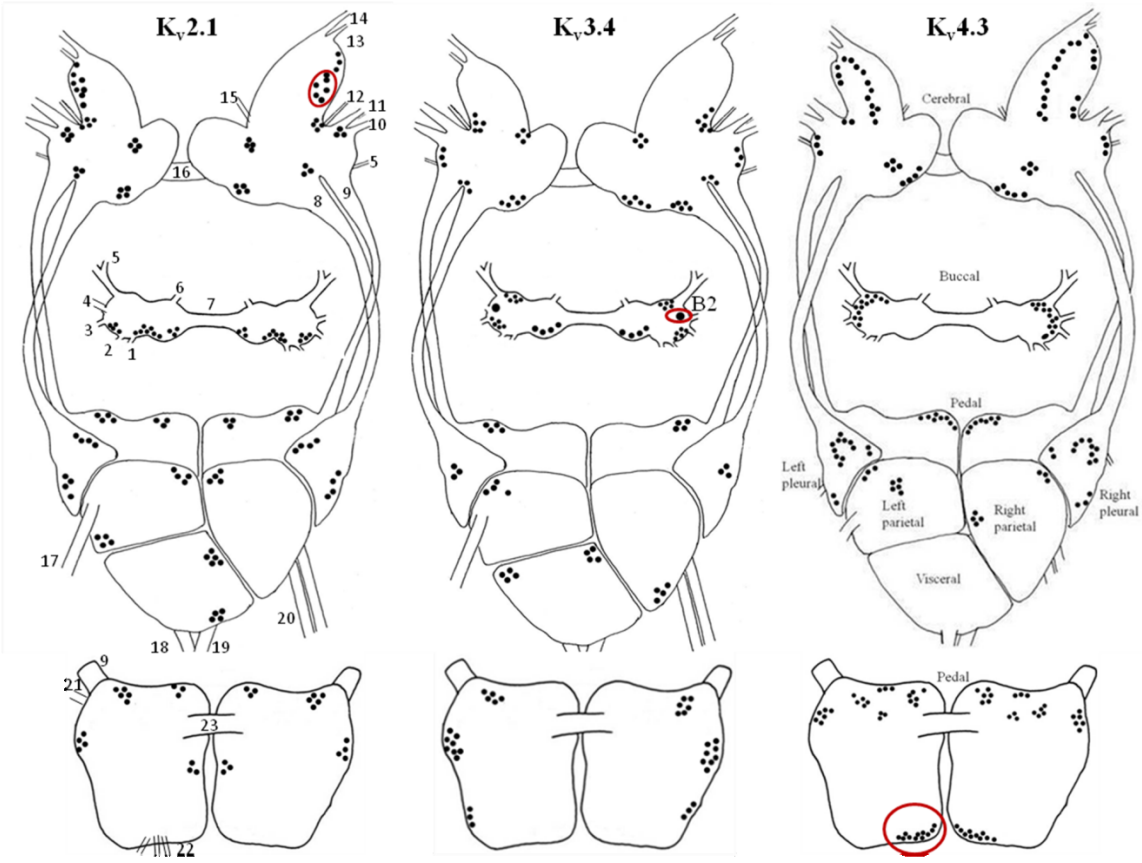
Kv2.1
Kv3.4
Kv4.3
Cerebral
Buccal
Pedal
Left pleural
Left parietal
Right parietal
Right pleural
Visceral
Pedal
B2

Fig. 5

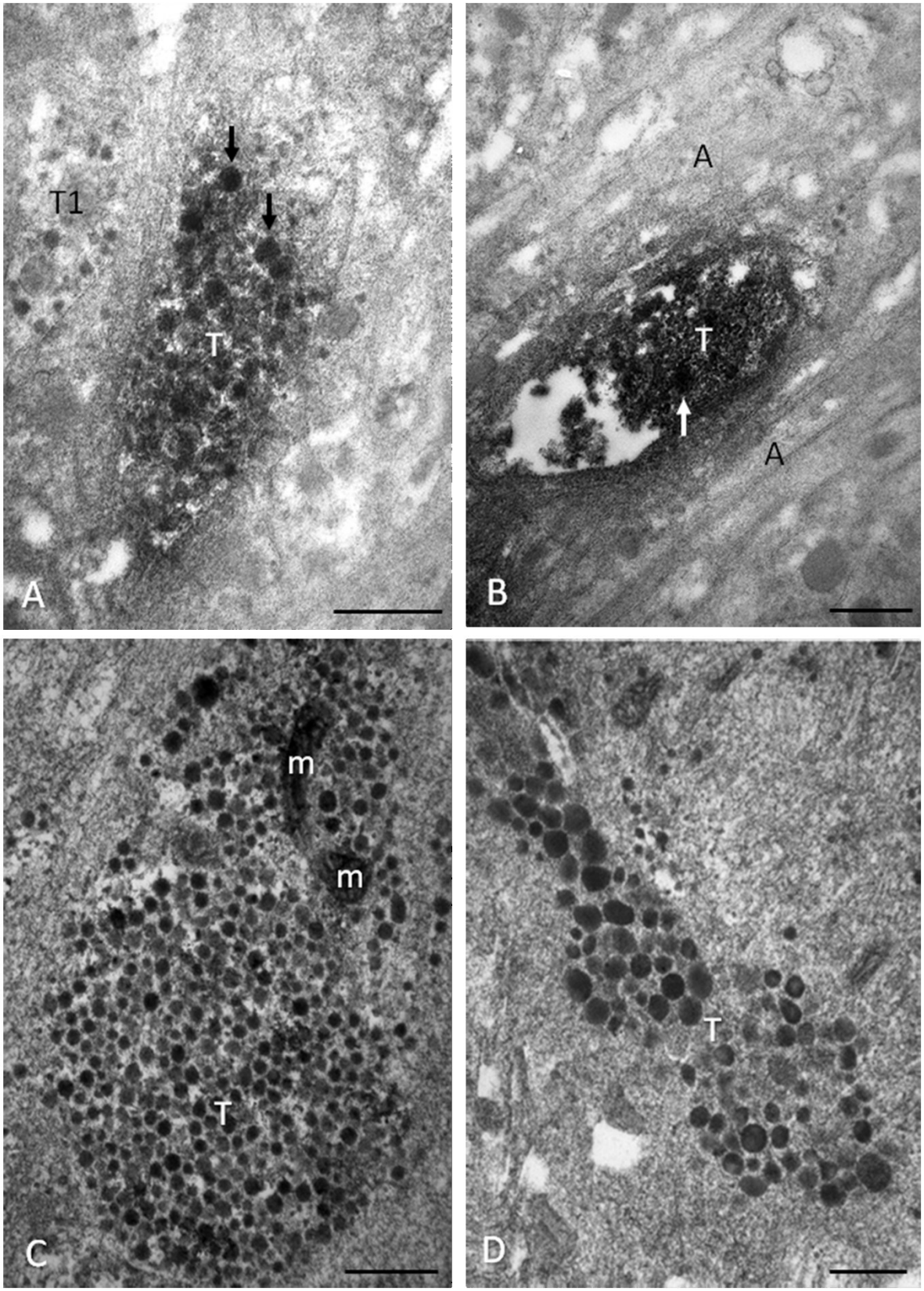

Fig. 6

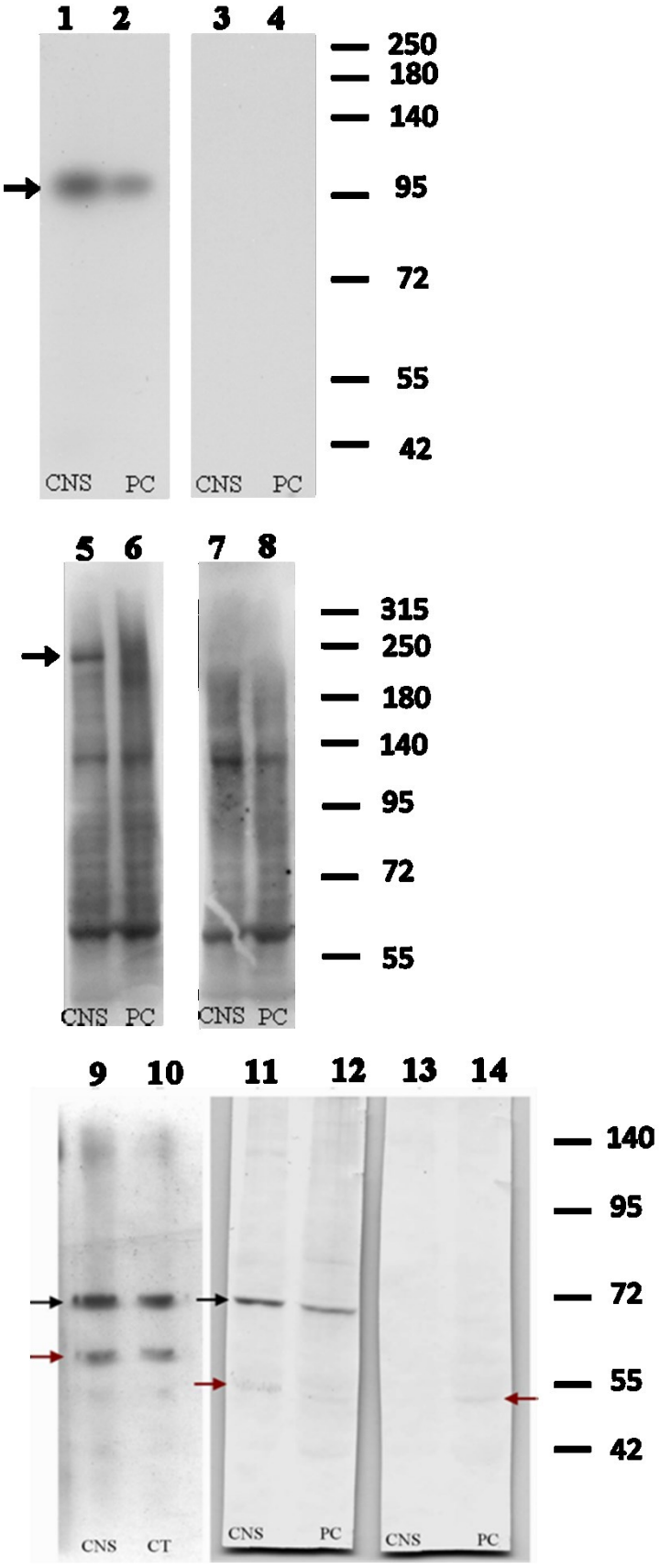
1 2
3 4
250
180
140
95
72
55
42
CNS PC
CNS PC
5 6
7 8
315
250
180
140
95
72
55
CNS PC
CNS PC
9 10
11 12
13 14
140
95
72
55
42
CNS CT
CNS PC
CNS PC

Fig. 7

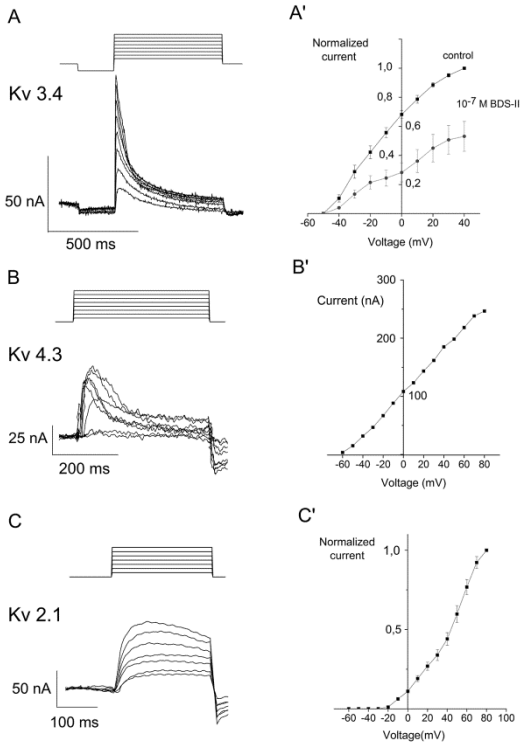
A
Kv 3.4
50 nA
500 ms
A'
Normalized current
control
10-7 M BDS-II
Voltage (mV)
B
Kv 4.3
25 nA
200 ms
B'
Current (nA)
Voltage (mV)
C
Kv 2.1
50 nA
100 ms
C'
Normalized current
Voltage(mV)

Fig. 8

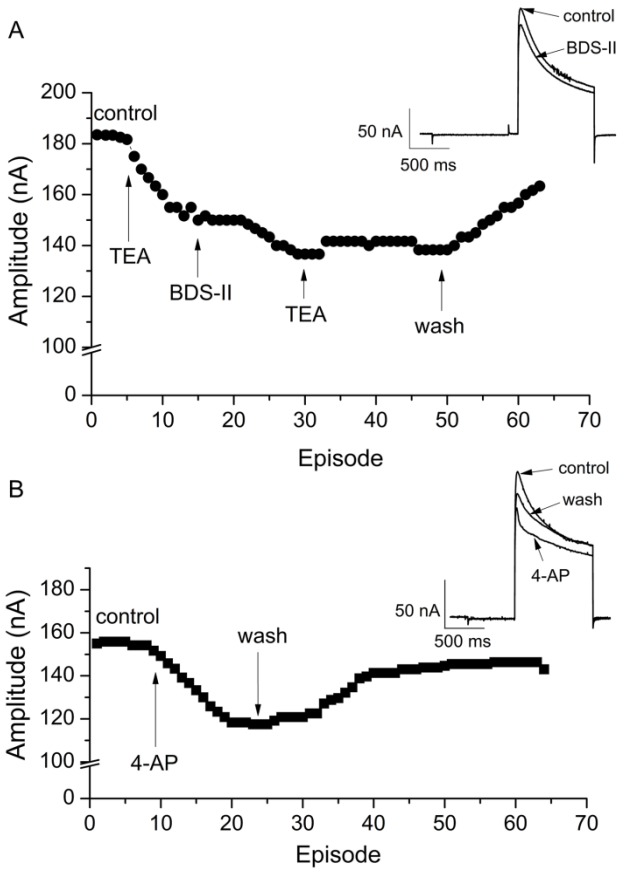
A
control
BDS-II
50 nA
500 ms
Amplitude (nA)
TEA
BDS-II
TEA
wash
Episode
B
control
wash
4-AP
50 nA
500 ms
Amplitude (nA)
control
wash
4-AP
Episode

Fig. 9